OCT4 activates a Suv39h1-repressive antisense lncRNA to couple histone H3 Lysine 9 methylation to pluripotency

Laure D Bernard, Agnès Dubois, Victor Heurtier, Véronique Fischer, Inma Gonzalez, Almira Chervova, Alexandra Tachtsidi, Noa Gil, Nick Owens, Lawrence E Bates, et al.

OCT4 activates a *Suv39h1*-repressive antisense lncRNA to couple histone H3 Lysine 9 methylation to pluripotency

Laure D. Bernard[1,2], Agnès Dubois[1], Victor Heurtier[1,2], Véronique Fischer[1], Inma Gonzalez[1], Almira Chervova[1], Alexandra Tachtsidi[1,2], Noa Gil[3,4], Nick Owens[1,5], Lawrence E. Bates[6], Sandrine Vandormael-Pournin[1], José C. R. Silva[7], Igor Ulitsky[3], Michel Cohen-Tannoudji[1], and Pablo Navarro[1,*]

1: Epigenomics, Proliferation, and the Identity of Cells, Department of Developmental and Stem Cell Biology, Institut Pasteur, CNRS UMR3738, 75015 Paris, France

2: Sorbonne Université, Collège doctoral, F-75005 Paris, France

3: Department of Immunology and Regenerative Biology and Department of Molecular Neuroscience, Weizmann Institute of Science, Rehovot, Israel

4: Current address: Friedrich Miescher Institute for Biomedical Research, Basel, Switzerland

5: Current address: Institute of Biomedical and Clinical Science, University of Exeter Medical School, Exeter, UK

6: MRC Human Genetics Unit, MRC Institute of Genetics and Cancer, University of Edinburgh, Edinburgh EH4 2XU, UK

7: Guangzhou Laboratory, Guangzhou International Bio Island, Guangzhou 510005, Guangdong Province, China

***: correspondence to pnavarro@pasteur.fr**

Abstract

Histone H3 Lysine 9 (H3K9) methylation, a characteristic mark of heterochromatin, is progressively implemented during development to contribute to cell fate restriction as differentiation proceeds. Accordingly, in undifferentiated and pluripotent mouse Embryonic Stem (ES) cells the global levels of H3K9 methylation are rather low and increase only upon differentiation. How global H3K9 methylation levels are coupled with the loss of pluripotency remains largely unknown. Here, we identify SUV39H1, a major H3K9 di- and tri-methylase, as an indirect target of the pluripotency network of Transcription Factors (TFs). We find that pluripotency TFs, principally OCT4, activate the expression of *Suv39h1as*, an antisense long non-coding RNA to *Suv39h1*. In turn, *Suv39h1as* downregulates *Suv39h1* transcription in cis via a mechanism involving the modulation of the chromatin status of the locus. The targeted deletion of the *Suv39h1as* promoter region triggers increased SUV39H1 expression and H3K9me2 and H3K9me3 levels, affecting all heterochromatic regions, particularly peri-centromeric major satellites and retrotransposons. This increase in heterochromatinization efficiency leads to accelerated and more efficient commitment into differentiation. We report, therefore, a simple genetic circuitry coupling the genetic control of pluripotency with the global efficiency of H3K9 methylation associated with a major cell fate restriction, the irreversible loss of pluripotency.

Introduction

During development, the establishment and maintenance of distinct gene expression patterns supporting the identity of each cell type are closely linked to the regulation of chromatin states[1]. Two broad states have been clearly and unambiguously identified: euchromatin, associated with transcriptionally active regions, and heterochromatin, associated with gene repression[2-5]. Two major states of heterochromatin have been traditionally considered. Facultative heterochromatin refers to a repressive chromatin environment displaying high variability across developmental stages, cell types and cell states. Indeed, silent developmental genes are usually embedded in facultative heterochromatin[3,5]. In contrast, ubiquitously silent elements such as retrotransposons and pericentromeric regions are locked by constitutive heterochromatin[4,5]. These two types of heterochromatin have been thought to be distinguishable by several molecular signatures, with facultative heterochromatin being characterized by trimethylation of histone H3 lysine 27 (H3K27me3) and constitutive heterochromatin by H3K9me3, among other chromatin features[2-5]. Nevertheless, recent data has challenged these strict definitions[3]. On the one hand, constitutive heterochromatin can under some circumstances be transcribed or decorated by marks previously associated with facultative heterochromatin[6-8]. On the other, while H3K27me3 and H3K9me2 were considered as major repressive mark for developmental genes, an increasing body of evidence points to H3K9me3 as an additional mean to silence developmental regulators as their expression is definitely shut down in particular lineages[9]. Hence, even though the role of H3K9 methylation in genome stability is unquestionable[10], its importance in gene regulatory mechanisms during development appears to be equally important. Indeed, mouse knock-out (KO) models of H3K9 histone methyltransferases (HMTs) display penetrant phenotypes, particularly during gastrulation when pluripotency is lost and major differentiation events take place[11,12]. Conversely, before reaching pluripotency during early mouse embryogenesis, the levels of H3K9 methylation are strictly controlled; promoting their increase, for instance by overexpressing the HMT SUV39H1, leads to developmental defects at the compaction stage[13,14].

While extensive research has contributed to our understanding of how the establishment and maintenance of H3K27me3 regulates developmental transitions[1-10], how the levels of H3K9 methylation are developmentally regulated is less clear. Yet, a major distinction has been identified, particularly using pluripotent cells such as mouse Embryonic Stem (ES) cells. Indeed, H3K27me3 characterizes developmental genes even before differentiation, when they are embedded in the so-called bivalent chromatin, which is simultaneously enriched for H3K27me3 and for marks of activity[15]. Upon differentiation, H3K27me3 is either consolidated or erased in a cell-type-dependent manner[16]. On the contrary, H3K9 methylation is more largely controlled at the level of its abundance: during

differentiation the global levels of H3K9me2 and H3K9me3 increase drastically[17,18]. Conversely, during the induction of pluripotency in vitro through reprogramming processes, H3K9 methylation has been shown to act as a major epigenetic barrier that is in part overcome by globally reducing its levels[18,19]. Therefore, while H3K27 methylation is mainly controlled by altering its genomic distribution, the global levels of H3K9 methylation display correlated changes to the differentiation status. Beyond the role of H3K9 methylation to stabilise somatic cell identities[20], how its global levels are seemingly coupled to the acquisition and loss of pluripotency, and what consequences this coupling has, remain open questions.

In this study, we aimed at understanding the molecular basis of the link between H3K9 methylation and pluripotency. We find *Suv39h1* to be the only HMT tightly connected to the network of transcription factors (TFs) supporting pluripotency, particularly to its main player *Oct4*. The analysis of the mechanisms of *Suv39h1* repression by OCT4 led us to identify *Suv39h1as*[21] as a *Suv39h1*-repressive antisense long non-coding RNA (lncRNA[22]) directly activated by OCT4. Using CRISPR-Cas9 mediated deletion of the antisense promoters, we further show that its activity controls the efficiency of H3K9 methylation in ES cells and the timing of commitment into differentiation. Thus, our work identifies a simple genetic network that provides a mechanistic perspective into how the global levels of H3K9 methylation are regulated at the onset of differentiation to irreversibly exit pluripotency.

Results

Suv39h1 expression is under the control of OCT4 in ES cells.

Using immunofluorescence, we first confirmed that differentiation of ES cells by LIF withdrawal leads to an increase of both H3K9me2 and H3K9me3, an increase that can also be observed in spontaneously differentiating cells in regular ES cell cultures, which express low levels of the pluripotency TFs OCT4 or NANOG (Fig.1A and Fig.S1A,B). Therefore, we hypothesized that one or several histone methyl-transferases or lysine demethylases (HMTs and KDMs, respectively)[2,4] could be directly controlled by pluripotency TFs and differentially expressed upon differentiation, linking the loss of pluripotency to increased H3K9 methylation. To assess this, we monitored mRNA levels of HMTs and KDMs using published RNA-seq datasets of undifferentiated and differentiating ES cells[23] (Fig.1B, Fig.S1C, Table S1). We found three HMTs to be upregulated upon differentiation: *Suv39h1*, *Suv39h2* and *Glp*. In contrast, all tested KDM displayed minor changes below 2-fold (Fig.S1C). We reasoned that the increase of *Suv39h1*, *Suv39h2* and *Glp* expression could either be due to a direct control of their transcription by pluripotency TFs or to alternative, indirect, mechanisms. To address this, we assessed the impact of the loss of individual pluripotency TFs (*Oct4*, *Nanog* and *Esrrb*) using dox-inducible knock-outs[24-26] (Fig.S1D). For NANOG, we used available datasets[23]; for OCT4 and ESRRB they were generated for this study (Table S1). Only one HMT, *Suv39h1*, was found upregulated 24h after inducing the loss of pluripotency TFs, particularly of OCT4, which depletion leads to a 2-fold increase in *Suv39h1* mRNA levels (Fig.1B). Moreover, analysis of datasets from gastrulating mouse embryos[27] also showed *Suv39h1* to be the only HMT to be upregulated upon differentiation of the three main germ layers (Fig.S1E). Hence, after confirming *Suv39h1* expression changes by RT-qPCR (Fig.S1F), we hypothesized that OCT4 may act as a repressor of *Suv39h1* expression to maintain low levels of H3K9 methylation until the onset of differentiation. Exploration of available ChIP-seq datasets[28] (Fig.1C) and direct validation by ChIP-qPCR (Fig.S1G) identified a hotspot of pluripotency TFs, including OCT4, in the vicinity of *Suv39h1*. However, this TF binding hotspot was found located 3' to *Suv39h1*, at around 27 kb of its promoter region. Notably, we noticed that this region coincides with the promoter region of an uncharacterized gene, *Gm14820* (*AK010638*), antisense to and largely overlapping *Suv39h1* (top of Fig.1C). This antisense transcript, *Suv39h1as*, has been previously identified in oocytes and suggested to oppose to *Suv39h1* expression at the oocyte to zygote transition[21].

Suv39h1as is an antisense long non-coding RNA.

Stranded, total RNA-seq confirmed *Suv39h1as* to be expressed in ES cells, at levels comparable to *Suv39h1* (Fig.1D). Using de novo transcript assembly with all the RNA-seq datasets presented in Table S1, together with direct cDNA cloning, sequencing and RT-qPCR, we identified several isoforms

expressed in ES cells (Fig.1E and Fig.S2A,B,C). All isoforms initiate from two distinct promoters, located in proximity to the region bound by pluripotency TFs, exhibit overlapping exons with *Suv39h1* and terminate within *Suv39h1* or in the vicinity of its 5' end. Notably, *Suv39h1as* is annotated as a long non-coding RNA (lncRNA). Accordingly, using two different algorithms (CPAT[29] and CPC2[30]), the nearly absent coding potential of all *Suv39h1as* isoforms was confirmed (Fig.1E). To further characterize *Suv39h1as*, we assessed the stability of its RNA products and found the half-life of its spliced and unspliced forms to be around 12h and 1h30, respectively (Fig.2A). However, *Suv39h1as* splicing is relatively inefficient compared to *Suv39h1* or another protein coding gene, *Nanog* (Fig.2B), as is generally the case for lncRNA[22]. Moreover, *Suv39h1as* was efficiently captured in poly-A selected RNA-seq, suggesting it is normally poly-adenylated (Table S1). Next, we aimed at visualizing *Suv39h1as* RNA molecules in single cells. For this, we designed oligonucleotides targeting *Suv39h1as* exons and performed strand-specific single molecule RNA-FISH (smFISH) coupled to DNA-FISH to identify the *Suv39h1as*/*Suv39h1* locus, using a fosmid covering the whole region (Fig.2C). We observed that *Suv39h1as* is mainly detected as a bright point in the nucleus, likely representing actively transcribed loci as it coincides with the DNA-FISH signal. A small number of single *Suv39h1as* RNA molecules could also be detected diffusing in the nucleus and, more rarely, in the cytoplasm. Quantification of the smFISH/DNA-FISH suggested a transcriptional frequency of around 50% in the population, with a median of 6 freely diffusing RNAs in cells presenting a transcriptionally active locus (Fig.2E). Hence, we conclude that the pluripotency TFs bind close to the two promoters of a *Suv39h1* antisense lncRNA, which is mostly localised at its site of transcription, poly-adenylated and poorly spliced even though the spliced isoforms are relatively stable. *Suv39h1as* is, moreover, conserved in humans (Fig.S2D).

Anticorrelated expression patterns of *Suv39h1* and *Suv39h1as*.

To investigate *Suv39h1as* and *Suv39h1* expression patterns at the single cell level, we designed oligonucleotides across *Suv39h1* exons and introns to monitor *Suv39h1*/*Suv39h1as* expression by smFISH in parallel to DNA-FISH (Fig. 2D). We found around 20% of cells actively transcribing both sense/antisense genes and around 30% transcribing either one or the other. Moreover, cells actively transcribing *Suv39h1as* displayed significantly fewer *Suv39h1* mRNA molecules (Fig. 2E). Next, we differentiated ES cells using three independent protocols based on LIF withdrawal, N2B27 or EpiLC-directed differentiation. These three assays showed a strong reduction of *Suv39h1as* expression after 3 days of differentiation, when *Suv39h1* expression increases (Fig.2F). Moreover, exploration of published RNA-seq during early embryogenesis[31,32] confirmed the anticorrelated expression patterns of *Suv39h1*/*Suv39h1as* during key events (Fig.2G): first, following fertilization (as previously suggested[21]), when *Suv39h1as* is highly expressed but decreases rapidly followed by *Suv39h1* upregulation; second in the pluripotent ICM when *Suv39h1as* peaks at high levels, coinciding with a

transient downregulation of *Suv39h1*. Hence, both *ex vivo* and *in vivo*, we observe anti-correlated expression dynamics of *Suv39h1*/*Suv39h1as*. Finally, to address whether *Suv39h1as* responds to OCT4 levels, we measured both RNA levels upon OCT4 depletion. We observed that the depletion of OCT4 leads to downregulation of *Suv39h1as*, reaching minimal levels of expression within 12h and accompanied by a marked increase of *Suv39h1* expression that reached maximal levels after 24h (Fig.2H). Analysis of published nuclear RNA-seq[33] further confirmed this observation, underscoring a dramatic transcriptional silencing of *Suv39h1as* upon OCT4 depletion and a strong transcriptional induction of *Suv39h1* (Fig.2I). Overall, *Suv39h1* and *Suv39h1as* display anticorrelated transcription levels upon differentiation and during early embryogenesis. This anticorrelation stems from single cell dynamics where the transcription of the antisense is accompanied by a reduction of the transcriptional frequency of *Suv39h1*. Since *Suv39h1as* is downregulated upon differentiation and upon the loss of OCT4, our data suggests that pluripotent TFs activate *Suv39h1as* transcription which, in turn, downregulates *Suv39h1* expression.

The *Oct4-Suv39h1as-Suv39h1* circuitry.

OCT4 depletion leads to *Suv39h1as* silencing within 12h (Fig.2H). However, to establish that this response is a primary effect mediated by OCT4 we aimed at analysing the effect of shorter OCT4 depletion. Using the same dox-inducible cells, we initially observed that *Suv39h1as* transcription assessed by unspliced RNA quantification starts to decrease as soon as 4h after inducing OCT4 loss (Fig.3A, left). This prompted us to use a faster degradation system of OCT4, generated by fusion with an IAA-inducible degron[34]. We observed a fast response of *Suv39h1as*, displaying a marked reduction of transcription as early as 2h after inducing OCT4 depletion (Fig.3A, right). In both systems, we observed that the loss of *Suv39h1as* transcription was followed by a nearly concomitant reduction of *Suv39h1as* mature RNA and an increase of *Suv39h1* mRNA. Hence, these analyses establish that *Suv39h1as* transcription responds rapidly to the loss of OCT4. This strengthens the notion that *Suv39h1as* is a direct OCT4 target that downregulates *Suv39h1* expression. To functionally establish the relationships between OCT4, *Suv39h1as*, *Suv39h1* and H3K9 methylation, we designed two gRNAs to delete 5,5kb encompassing the two promoters of *Suv39h1as*. Two independent KO clones, A8 and D8, were generated (Fig.S3). RT-qPCR showed a complete extinction of *Suv39h1as* expression (Fig.3B). We then addressed the impact of *Suv39h1as* depletion on *Suv39h1* expression, both before and during differentiation. In the two mutant clones we observed an increase of *Suv39h1* expression in undifferentiated cells, reaching the levels observed upon differentiation in wild-type (WT) cells (Fig.3B). In differentiating cells, when *Suv39h1as* is naturally silenced and OCT4 binding at its promoter abrogated (Fig.S4A), the deletion had no impact (Fig.3B), as expected. Analysis of several differentiation markers (Fig.S4B, left) ruled out the possibility that differences in *Suv39h1* expression

derive from indirect consequences linked to the differentiation status of the cells, as already suggested by the fast response of *Suv39h1as* transcription to OCT4 depletion (Fig.3A). Moreover, these results were independent of the differentiation protocol (Fig.S4C). Therefore, these results indicate that *Suv39h1as* acts as a pluripotency-associated repressor of *Suv39h1* expression. To more directly address whether OCT4 represses *Suv39h1* expression via *Suv39h1as*, we used siRNAs targeting *Oct4* to test whether in the absence of *Suv39h1as*, the loss of OCT4 would lead to any modification of *Suv39h1* expression. Whereas in WT cells the knock-down of *Oct4* (above 80% efficiency, Fig.S4D) led to higher *Suv39h1* expression, in mutant cells it was fully inconsequential (Fig.3C). Other OCT4-responsive genes, such as *Cdx2*[25], displayed similar changes in WT and mutant cells upon *Oct4* knock-down (Fig.S4B, middle panel). Thus, OCT4-dependent repression of *Suv39h1* only occurs in the presence of the promoter region of *Suv39h1as*, suggesting that it requires *Suv39h1as* transcription. Next, we performed smFISH to study *Suv39h1* upregulation with single cell resolution (Fig.3D). We observed a marked increase in the transcriptional frequency of *Suv39h1*, rising from 47.6% in WT to 76.3% and 74.1% in A8 and D8, respectively. Moreover, the number of *Suv39h1* mRNAs per cell also increased substantially, with virtually no cell displaying an absence of *Suv39h1* mRNAs (Fig.3E). This increase in *Suv39h1* transcription in mutant cells was accompanied by higher levels of SUV39H1 protein levels, reaching those observed in WT differentiating cells (Fig.3F). Altogether, our results indicate that OCT4 directly activates *Suv39h1as* transcription, which in turn transcriptionally downregulates *Suv39h1*, leading to reduced mRNA and protein levels. This simple genetic circuitry ensures increased SUV39H1 expression during differentiation.

Suv39h1as modifies the chromatin of the _Suv39h1as_/_Suv39h1_ locus.

We have observed that in mutant ES cells lacking *Suv39h1as* expression, the transcriptional frequency of *Suv39h1* increases from 50 to 75% (Fig.3D). Similarly, upon OCT4 depletion *Suv39h1* pre-mRNA increases substantially (Fig. 2I) and rapidly (Fig. 3A). Moreover, the absence of *Suv39h1as* is not accompanied by increased stability of *Suv39h1* mRNAs (Fig.S5A). In contrast, in *Suv39h1as* mutant cells we observed increased chromatin accessibility of the *Suv39h1* promoter region (Fig.S5B and Table S2). Therefore, *Suv39h1as* is likely to act as a transcriptional repressor of *Suv39h1*. To explore this, and given that other antisense transcription units have been shown to modify the chromatin of their corresponding sense gene[35-37], we used a ChIP approach to establish the histone modification profile of the locus (Fig.4). First, we monitored H3K4 methylation profiles. We found H3K4me1/me2, which usually mark transcriptionally competent regions[38], to globally decorate the locus with minimal focal accumulation at promoters. Conversely, H3K4me3, a mark of activity[38], was focally enriched at the *Suv39h1* promoter and displayed low levels over the antisense promoter. We then profiled the active histone acetylation marks H3K9ac and H3K27ac. Similarly to H3K4me3, we found H3K9ac to

preferentially mark the *Suv39h1* promoter. In contrast, both sense and antisense gene promoters where enriched for H3K27ac. In mutant cells, we observed a global decrease of H3K4me1/me2 over the region transcribed by *Suv39h1as*, particularly before it reaches the *Suv39h1* gene body (Fig.4), indicating its transcription promotes the establishment of these marks. The lack of H3K4me1/me2 reduction within the region transcribed by both genes suggests that the increased transcription of *Suv39h1* may have a compensatory role. Moreover, H3K4me2, H3K9ac and H3K27ac, all marks of gene activity, showed a slight but statistically significant increase at the *Suv39h1* promoter in the absence of *Suv39h1as* (Fig.4). Altogether, this analysis suggests that the loss of *Suv39h1as* leads to increased *Suv39h1* transcription at least in part mediated by increased euchromatinisation and accessibility of the *Suv39h1* promoter. While undeniably small, the effects of the loss of *Suv39h1as* on the *Suv39h1* promoter can be reproduced with different assays measuring chromatin activity.

Global increase of H3K9me2 and H3K9me3 in *Suv39h1as* mutant ES cells.

The absence of *Suv39h1as* transcription in ES cells leads to increased SUV39H1 protein levels (Fig.3F), as confirmed by immuno-fluorescence: heterochromatic regions such as chromocenters prominently accumulate SUV39H1 in mutant cells (Fig.5A, Fig.S6A). Consequently, in both mutant clones we observed higher levels of H3K9me2 and H3K9me3 (Fig.5B left panel), similar to those observed in WT differentiating cells (Fig.S6B), establishing a direct link between *Suv39h1as* and the global levels of H3K9 methylation in ES cells. According to the preferential enrichment of SUV39H1 at chromocenters, where H3K9me3-enriched peri-centromeric heterochromatin clusters[4], the increase of H3K9me3 in *Suv39h1as* mutant cells was higher than that of H3K9me2 (Fig.5B left panel). Hence, we aimed at more precisely characterise H3K9me3 in WT and *Suv39h1as* mutant cells by ChIP-seq. We identified 48,584 regions with more than 3-fold enrichment of H3K9me3 compared to the corresponding input in either WT or in at least one mutant clone (Table S3). Comparative analysis of WT and mutant cells showed that the vast majority of these regions display higher H3K9me3 enrichment in the absence of *Suv39h1as* (Fig.5C), in magnitudes similar to those observed by immuno-fluorescence (Fig.5B right panel). We also observed that more than 80% of H3K9me3-enriched regions overlap with retrotransposons (either LTRs, LINEs, or both; Fig.5D) and only minimally with cis regulatory elements (cRE in Fig.5D), as previously showed[7]. Next, we quantified the effect of *Suv39h1as* KO at repetitive elements. We observed a strong bias towards a global and moderate increase of H3K9me3 over a multitude of families (Fig.5E, Table S4), most notably at major satellites of peri-centromeric regions (red dot in the left panel of Fig.5E and Fig.S6C), but also at retrotransposons such as LINE L1s or LTRs (ERVKs and ERVLs; Fig.5E and Fig.S6D). We conclude that *Suv39h1as* mutant cells display increased efficiency to trigger heterochromatin in ES cells.

The lack of *Suv39h1as* leads to accelerated differentiation commitment.

We finally wondered whether the increase of H3K9 methylation taking place in *Suv39h1as* mutant cells had any physiological impact. First, we used clonal assays to assess self-renewal and differentiation efficiency (Fig.6A,B). Either in conditions of reinforced self-renewal (2i/LIF), in traditional serum-containing culture medium (FCS/LIF) or in the absence of LIF (FCS), the number of alkaline-phosphatase colonies, a marker of pluripotent cells, was similar between WT and mutant clones. Hence, the presence of increased H3K9 methylation is largely inconsequential for self-renewal and for the loss of pluripotency. In agreement, both WT and mutant cells proliferate and differentiate normally, as evaluated morphologically (Fig.S7A) and by marker expression (Fig.S7B and Fig.S4B). However, during differentiation, the role of H3K9 methylation is to restrict cell fate and developmental competence[9,18,39,40], more than to elicit differentiation, with SUV39H1 playing a preponderant role in lineage-dependent maintenance of gene silencing in somatic cells[41]. Therefore, we reasoned that the loss of *Suv39h1as* could modulate the timing of commitment into differentiation. To test this, we used an established assay[42] whereby WT and mutant clones were differentiated in parallel and, every day, the cells were harvested and reseeded clonally in 2i/LIF: only those cells that were not yet committed into irreversible differentiation can self-renew and form undifferentiated colonies (Fig.6C,D). As previously shown[42], we observed that commitment took place between days 2 and 3 in WT cells, with a reduction in clonogenicity of nearly 90% (Fig.6D). In mutant cells, however, the reduction in the number of undifferentiated colonies was more marked from day 2.5 onwards (Fig.6D). Therefore, the premature establishment of higher levels of H3K9me2/me3 in ES cells facilitates the irreversible commitment into differentiation, in line with the role of these repressive marks in locking cell fate changes[20].

Discussion

In this study, we have identified a genetic network linking the control of the global levels of H3K9 methylation to pluripotency. The pluripotency network, mainly through OCT4, activates *Suv39h1as*, an antisense lncRNA to the *Suv39h1* gene; in turn, *Suv39h1as* represses *Suv39h1* expression. Consequently, the level of H3K9 methylation is reduced. Upon differentiation, the collapse of the pluripotency network leads to the silencing of *Suv39h1as*, enabling increased SUV39H1 expression and H3K9 methylation, which affects the timing and efficiency of the irreversible commitment into differentiation. Given the lack of strong effects at a small number of defined regulators of differentiation in *Suv39h1as* mutant cells, our data suggest that their faster commitment into differentiation is achieved by globally ameliorating the efficiency of H3K9 methylation, as illustrated by higher levels of H3K9me3 at peri-centromeric major satellites and at retrotransposons. During exit from pluripotency, when proper epigenetic silencing is implemented[43], the enhancement of heterochromatinization may enable the long-term changes of gene expression required to acquire new cell identities. Moreover, it is noteworthy that the *Oct4-Suv39h1as-Suv39h1* genetic axis may also act as a time-delay generator, enabling ES cells to filter out transient and short fluctuations of the pluripotency network[44]: only a long decrease in activity of pluripotency TFs, such as that occurring during the exit from pluripotency, may be sufficient to elicit the increase in SUV39H1 expression that will follow the extinction of *Suv39h1as*.

Antisense lncRNAs are frequent in mammals, with 29% of canonical protein coding genes displaying antisense transcription[45]. Given their antisense orientation and the resulting complementarity, antisense lncRNAs can theoretically regulate their cis-linked sense gene through a wide variety of mechanisms. By deleting the *Suv39h1as* promoter region, we found that *Suv39h1as* controls the transcriptional frequency of *Suv39h1*, whose promoter becomes more accessible and enriched in euchromatin marks. Additionally, *Suv39h1as* mutants display no changes of *Suv39h1* mRNA stability. Moreover, OCT4 depletion leads to a fast silencing of *Suv39h1as*, accompanied by a transcriptional induction of *Suv39h1* that takes place almost concomitantly to the decrease of mature *Suv39h1as* RNA. Altogether, this data supports the notion of a transcriptional control of the *Suv39h1* promoter by *Suv39h1as*, either by the act of *Suv39h1as* transcription itself or through mechanisms involving the unspliced *Suv39h1as* RNA. Notably, this ambiguity characterises other well-known pairs of sense/antisense genes, such as *Xist*/*Tsix*[35-37]. Like the loss of *Tsix*, that of *Suv39h1as* results in complex chromatin changes, which suggest that *Suv39h1as* triggers H3K4me1 and me2 throughout the locus and, at the same time, reduces the enrichment for active histone marks and the accessibility of the *Suv39h1* promoter. Even though the reminiscence of these effects to those triggered by *Tsix* are striking, possibly revealing a general property of antisense transcription, we cannot exclude that they

are indirect consequences of a transcriptional induction of *Suv39h1* mediated by other mechanisms. For instance, a direct competition between *Suv39h1*/*Suv39h1as* and other gene promoters for shared enhancers could play an important role[46]. In agreement, exploration of the topology of the extended *Suv39h1*/*Suv39h1as* locus suggests that the 3D organization is compatible with the involvement of 3D events (Fig.S8A); nevertheless, neither chromatin accessibility (Fig.S8B,C), nor expression analyses of genes previously identified[47] as sharing at least a common enhancer with *Suv39h1*/*Suv39h1as* (Fig.S8D), display any change in our mutant cells. This indicates that *Suv39h1as* has a very local and specific role within the locus: to control the promoter activity of *Suv39h1*. Nevertheless, other additional mechanisms cannot be excluded, such as direct collisions of the sense/antisense polymerases[48] or post-transcriptional mechanisms involving splicing[49].

The deletion of *Suv39h1as* promoter and the ensuing increase in H3K9 methylation appears to be largely tolerated by ES cells: they self-renew and differentiate efficiently. This observation is in line with others, where histone modifiers have been either invalidated or ectopically expressed in ES cells with minor consequences for self-renewal[50,51]. However, despite the fact that *Suv39h1as* mutant cells self-renew and differentiate normally, we asked whether the timing of commitment into differentiation is altered. Our results showed a faster and more efficient commitment into differentiation, suggesting that the global levels of H3K9 methylation contribute to irreversibly lock the loss of pluripotency. This observation adds to the notion of H3K9 methylation in general, and SUV39H1 in particular, acting as an epigenetic barrier providing robustness to cell fate changes[9,18,39:41]. Moreover, our results also underscore the dominance of pluripotency TFs over chromatin modifications[51]. We had already shown that NANOG, another key pluripotency TF, controls H3K27me3 levels, particularly during early differentiation[23]. Here, we complement this notion with OCT4 controlling H3K9me3 via the *Suv39h1as*/*Suv39h1* tandem. Together, these results place the control of the global levels of heterochromatin marks under the activity of the pluripotency network, extending the concept of the genetic dominance of pluripotency. Whether our observations and conclusions apply to early mouse embryogenesis and to the acquisition and loss of pluripotency in vivo is now a question of primary importance. Notably, H3K9 methylation levels are exquisitely regulated during early embryogenesis[52]. It is noteworthy that SUV39H1 is absent in oocytes and its expression starts at the 2-4 cell transition stage[31,32], when the reconfiguration of constitutive heterochromatin as chromocenters is initiated. Moreover, the overexpression of SUV39H1 during early embryogenesis leads to developmental defects[13,14]: its zygotic overexpression leads to a developmental arrest during compaction. Since *Suv39h1as* displays an exquisite anticorrelated expression to *Suv39h1* upon fertilization (as initially suggested[21] and our data reanalysis has confirmed), whether *Suv39h1as* holds *Suv39h1* expression until the appropriate time to enable the timely establishing of the first heterochromatic structures in the embryo, represents an important question for the future.

Methods:

Cell lines and generation of A8 and D8 *Suv39h1as* mutant cells.

WT cells in this study are E14Tg2a ES cells, from which all mutant cells were derived. Dox-inducible knock-out cells as well as OCT-AID cells have been previously described (*Esrrb*: EKOiE[24], *Oct4*: ZHBTC4[25], *Nanog*: 44iN[26], OCT-AID[34]). To generate ES cells deleted for the *Suv39h1as* promoter, a CRISPR-Cas9 approach was followed using gRNAs available in Table S5. Additional details are available in supplementary methods and in Fig.S4.

Regular cell culture and differentiation.

Cells were cultured at 37°C, 7% CO2 on gelatine-coated plates in either FCS/LIF or in 2i/LIF, as indicated, and passaged every 2-3 days. Cells cultured in FCS/LIF were differentiated by withdrawing LIF for 3 days. N2B27 and EpiLC differentiation assays were performed with cells cultured in 2i/LIF for a minimum of 3 passages, after which LIF and 2i were withdrawn (for both N2B27 and EpiLC) and activin A, FGF and KSR supplemented (for EpiLC only). All details are available in supplementary methods.

Commitment assays.

For commitment assays, 600 cells obtained every day of differentiation in N2B27 were plated in poly-L-ornithine/laminin-coated wells of a 6 wells plate, cultured for 7 days in 2i+LIF and stained for alkaline phosphatase activity (supplementary methods).

Immunostainings.

To ensure direct comparisons, cell lines or conditions to be compared were individually labelled either with Rhodamine Red or with Deep Red dyes. The labelled cells were then collected, mixed at a 1:1 ratio and seeded onto Poly-L-Ornithine/Laminin coated µ-slides. After 6 hours of culture at 37°C and 7% CO2, they were prepared for immunostaining and imaged. Additional details are available in supplementary methods.

Single molecule FISH and DNA-FISH.

Single-strand probes for *Suv39h1* (47 oligos, 30 in exons, see sequences Table S5) and *Suv39h1as* (35 exonic oligos, see sequences Table S5) were used for smFISH and the position of each image recorded on the microscope. Subsequently, DNA-FISH was performed with a labelled fosmid (WIBR1-2188H11 – from bacpac.chori.org) at the same positions (supplementary methods).

ChIP-seq and ATAC-seq.

Both assays and the corresponding libraries were performed and generated as previously described[28], with the exception that fixed Drosophila chromatin was spiked in to be used as an internal normaliser, and sequenced for 75 cycles in a NextSeq 500 (SR for ChIP-seq and PE for ATAC-seq). For ChIP-seq, adapters with UMIs to enable distinguishing true identical reads from PCR duplicates[28] were used to improve mapping of repetitive DNA. After alignment (Bowtie2) to both mouse and Drosophila genomes, mouse peaks were identified with MACS2 for ATAC-seq and with a previously described approach[40] for H3K9me3. Read counts at these regions were normalised to the total number of reads aligning to the Drosophila genome, considering for ChIP-seq both the ChIP and corresponding input of each replicate for H3K9me3. For ChIP-seq, for reads mapping at multiple positions only one was randomly kept; for ATAC-seq, all multi-mappers were excluded. Global analysis of repetitive elements was performed with RepEnrich[53] followed by DESeq2[55].

Datasets and availability.

All genome-wide datasets generated for this study are available in GEO (GSE184140): poly-A RNA-seq of EKOiE (GSM5578482 to GSM5578485) and ZHBTC4 cells (GSM5578486 to GSM5578489); total RNA-seq of E14Tg2a (GSM5578490 to GSM5578491). Other available datasets in GEO were used: from GSE118898 – GSM3350412 to GSM3350417 (44iN), GSM3350424, GSM3350426, GSM3350428 (undifferentiated cells), GSM3350429, GSM3350431, GSM3350433 (differentiating cells); from GSE87822 – GSM2341322 to GSM2341327 (nuclear RNA-seq in ZHBTC4); GSE121708 (single-cell RNA-seq of E4.5 and E7.5 embryos using processed data from: ftp://ftp.ebi.ac.uk/pub/databases/scnmt_gastrulation); GSE45719 (zygote to 16C early embryo single-cell RNA-seq) – GSM1112490 to GSM1112581, GSM1112603 to GSM1112610, GSM1112656 to GSM1112663, GSM1112694 to GSM1112705,

GSM1112766 to GSM1112769. Datasets available from ArrayExpres (EMBL-EBI) were also used: E-MTAB-2958 (RNA-seq of E2.5 to E4.5 mouse embryos).

Competing Interest Statement:

The authors declare no competing interest.

Acknowledgements: This study was conceived by P.N with inputs from L.B. and V.H. Experiments were designed and executed by L.B., with help from A.D., V.H., A.T., S.V-P. and M.C-T. RNA-seq analyses and assembly were done by N.G., N.O., A.C. and I.U. ChIP-seq was performed by V.F. and ATAC-seq by I.G; A.C. analysed them both. Auxin-inducible depletion experiments were done by L.E.B and J.C.R.S. The paper was written by L.B. and P.N. L.B. acknowledges the Ecole Normale Supérieure and Sorbonne Université for funding. P.N. and M.C-T. acknowledge the Labex Revive (Investissement d'Avenir; ANR-10-LABX-73), the Institut Pasteur and the CNRS for funding. P.N. acknowledges Elphège Nora for discussions on chromatin topology and all referees for constructive criticisms; in particular two referees that alerted the authors that *Suv39h1as* had already being identified by the Knowles lab in 2006.

Figures, Supplementary Figures and Supplementary Tables legends.

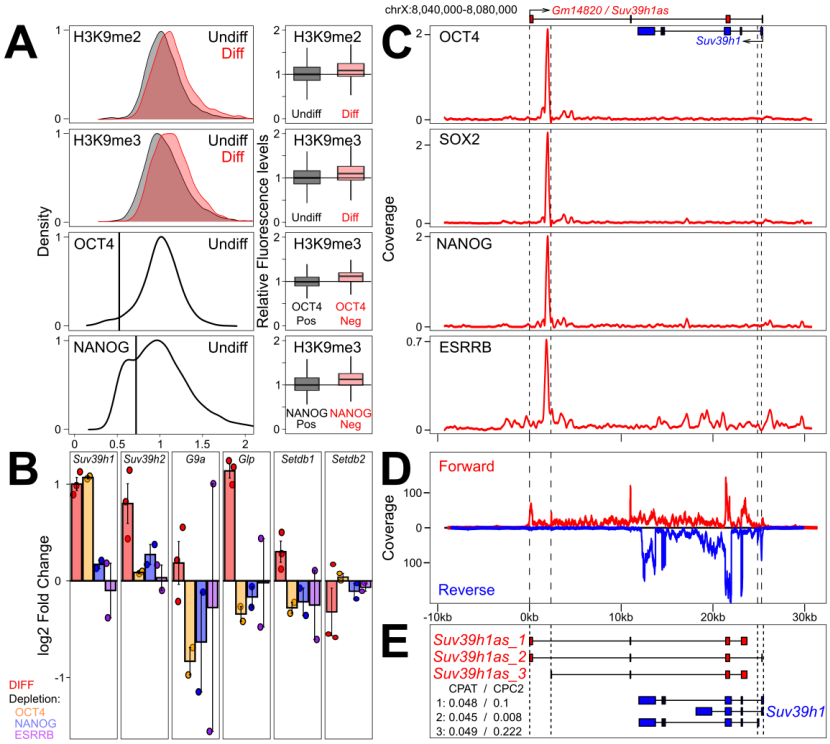

Figure 1: *Suv39h1* is downregulated by OCT4, which binds to the promoter of a *Suv39h1* antisense lncRNA, *Suv39h1as*. (A) On the left, distribution of H3K9me2, H3K9me3, OCT4 and NANOG in undifferentiated (black; n=4503, 3150, 3276 and 5615 cells, respectively) and differentiating (3d of LIF withdrawal – red; n=6231, 3755, respectively) ES cell populations assessed by immunofluorescence. On the right, boxplot corresponding to different populations shown on the left: for H3K9me2/me3 distributions, the boxplots compare undifferentiated and differentiating cells (KS test $p<10^{-15}$); for OCT4 and NANOG distributions, the boxplots compare H3K9me3 between positive/negative subpopulations of OCT4 or NANOG (vertical line on the left panels; KS test $p<10^{-15}$ for both TFs) **(B)** Log2 fold change of the indicated gene after differentiating ES cells as in (A) or 24h after inducing the depletion of individual TFs, as indicated, using Dox-inducible knock-out cells. Each dot represents an independent replicate and the bar and error bars the corresponding means and standard errors. *Suv39h1* upregulation upon differentiation or OCT4 depletion ($p<0.001$) and *Suv39h2* and *Glp* upregulation upon differentiation ($p<0.05$) are statistically significant (t test). **(C)** Average binding profile of OCT4, SOX2, NANOG and ESRRB (reads per million) across the *Suv39h1/Gm14820* locus (mm10, chrX:8,040,000-8,080,000). *Suv39h1* and *Gm14820/Suv39h1as* are schematically represented on top. **(D)** RNA-seq profile across the *Suv39h1/Suv39h1as* locus, with forward and reverse fragment counts expressed with positive and negative values. **(E)** Schematic representation of *Suv39h1as* (red) and *Suv39h1* (blue) isoforms as determined in Fig.S2. The coding probabilities calculated with CPAT and CPC2 algorithms are shown for the three isoforms of *Suv39h1as*. The vertical dashed lines in (C), (D) and (E) mark the position of *Suv39h1as* or *Suv39h1* promoters.

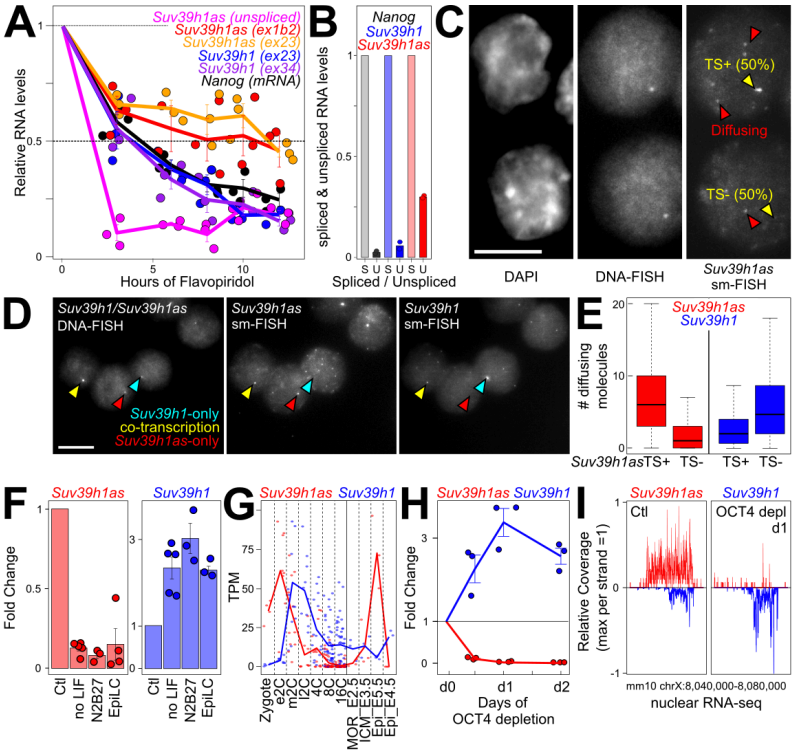

Figure 2: *Suv39h1as* is a nuclear, stable and lowly expressed lncRNA with anticorrelated expression dynamics to *Suv39h1*. (A) RT-qPCR analysis of the half-life of several RNA species during a transcription inhibition assay with Flavopiridol: *Suv39h1* mRNA, using two trans-exonic primer pairs between exons 2 and 3 (blue – ex23) or exons 3 and 4 (purple – ex34); *Suv39h1as*, using two trans-exonic primer pairs between exons 1b and 2 (red – ex1b2) or exons 2 and 3 (orange – ex23) or primer pairs amplifying the unspliced RNA (magenta – pre-mRNA); *Nanog* mRNA (black). Each dot represents an independent replicate and the line the corresponding mean and standard error. Ribosomal RNA (28s) was used for normalization. **(B)** Histogram representing unspliced RNA levels relative to corresponding spliced RNAs for *Nanog*, *Suv39h1* and *Suv39h1as*, as measured by RNA-seq. Each dot represents an independent replicate and the bar the corresponding mean. **(C)** Representative sm-FISH followed by DNA-FISH visualizing *Suv39h1as* RNA molecules and the *Suv39h1*/*Suv39h1as* locus, respectively, in undifferentiated WT cells. Red arrowheads indicate RNAs diffusing away from the locus, which is indicated by a yellow arrow. The proportion of actively transcribing cells is indicated (n=358 cells). **(D)** Representative sm-FISH of *Suv39h1as* and *Suv39h1* RNA molecules, followed by DNA-FISH visualising the *Suv39h1*/*Suv39h1as* locus in WT cells (n= 358). Selected loci transcribing either *Suv39h1*, *Suv39h1as* or both genes are indicated with arrow heads: blue, *Suv39h1*-only (30%); red, *Suv39h1as*-only (30%); yellow for cells transcribing both (20%). **(E)** Boxplots (median; 25-75% percentiles; error bars) showing the number of *Suv39h1* diffusible molecules counted in cells presenting an active (TS+) or inactive (TS-) *Suv39h1as* gene (n=358 WT cells). The increased of *Suv39h1* diffusing molecules in *Suv39h1*_TS- versus *Suv39h1as*_TS+ was assessed with KS test ($p<10^{-11}$). **(F)** Fold change expression of *Suv39h1as* (red) or *Suv39h1* (blue) measured by RT-qPCR in differentiating WT cells versus undifferentiated controls (ctl). Differentiation was triggered for three days with three independent protocols: LIF withdrawal from FCS/LIF cultures (no LIF), 2i and LIF withdrawal from 2i+LIF cultures (N2B27) or EpiLC differentiation from 2i+LIF cultures (EpiLC). Values were normalized to *Tbp* and fold changes calculated to their respective control cultures. Each dot represents an independent replicate and the bar and error bars the corresponding means and standard errors. Gene expression differences were assessed against the respective undifferentiated controls (t test $p<0.05$ for *Suv39h1* and $p<0.01$ for *Suv39h1as* for all differentiation assays). **(G)** Mean expression dynamics of *Suv39h1* and *Suv39h1as* in published RNA-seq datasets of early mouse embryogenesis (left part REF, Zygote to 16-cell stage[31]; right part, Morula, ICM and Epiblast[32]). **(H)** RT-qPCR analysis of *Suv39h1as* (red) and *Suv39h1* (blue) expression upon OCT4 depletion in ZHBTC4 cells treated with Dox for the indicated time. Values were normalized to *Tbp*. Each dot represents an independent replicate and the line the corresponding mean with standard errors. Each time-point was compared to untreated cells with a t test ($p<0.001$ for *Suv39h1as* and $p<0.05$ for *Suv39h1*). **(I)** Analysis of publicly available[33] nuclear RNA-seq over the *Suv39h1*/*Suv39h1as* locus in untreated and OCT4-depleted ZHBTC4 cells (1 day of Dox treatment), presented as in Fig.1D.

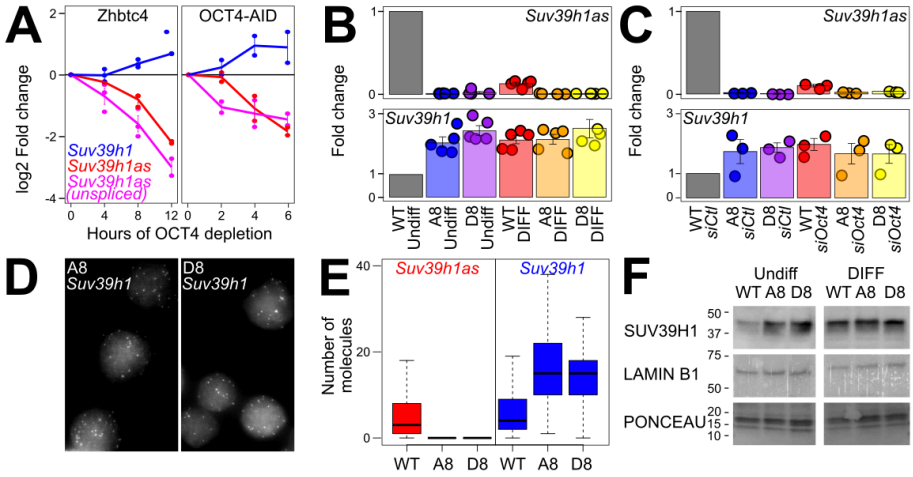

Figure 3: OCT4 represses *Suv39h1* via *Suv39h1as*. (A) Log2 expression fold change of *Suv39h1* (blue), *Suv39h1as* (red) and unspliced *Suv39h1as* (magenta) upon OCT4 depletion in ZHBTC4 (left) and OCT4-AID (right) cells. The X-axis shows the number of hours of treatment with Dox (ZHBTC4) and IAA (OCT4-AID). Two biological replicates per cell line and time-point are shown. The global effect of the treatments was assessed by comparing all time points together against untreated cells with a t test ($p<0.02$ for both ZHBTC4 and OCT4-AID). **(B)** Expression fold change of *Suv39h1as* (top) and *Suv39h1* (bottom) in WT and *Suv39h1as*-mutant cells (A8 and D8) cultured in undifferentiated or differentiating conditions (3 days without LIF). Values were normalized to *Tbp*. Each dot represents an independent replicate and the bar and error bars the corresponding means and standard errors. The increase of Suv39h1 in each clone versus WT cells was compared with a t test ($p=0.011$ and 0.0016 for A8 and D8, respectively). **(C)** Expression fold change of *Suv39h1as* (top) and *Suv39h1* (bottom) in WT and *Suv39h1as*-mutant cells (A8 and D8) knocked-down with either control or *Oct4*-targeted siRNAs. Values were normalized to *Tbp*. Each dot represents an independent replicate and the bar and error bars the corresponding means and standard errors. The increase of *Suv39h1* expression upon OCT4 knock-down was assessed against control siRNAs with a t test ($p=0.027$ in WT cells). **(D)** Representative sm-FISH images of *Suv39h1* in A8 and D8 cells (WT cells presented in Fig.2D). Differences in the frequency of active transcription sites were assessed with a Chi2 test ($p<10^{-10}$ for both clones against WT cells) **(E)** Boxplots (median; 25-75% percentiles; error bars) showing the number of *Suv39h1as* (red) or *Suv39h1* (blue) diffusible molecules counted in WT (n= 358) or mutant cells (A8, n= 289; D8, n= 270). Differences in the number of *Suv39h1* molecules were assessed with a Mann-Whitney test ($p<10^{-15}$ for both clones against WT cells). **(F)** Representative Western-Blot of SUV39H1, LAMIN B1 and corresponding Ponceau for WT and mutant cells (A8 and D8) in undifferentiated and differentiating (3 days without LIF) conditions. On the left of each image is indicated the protein scale in kDa.

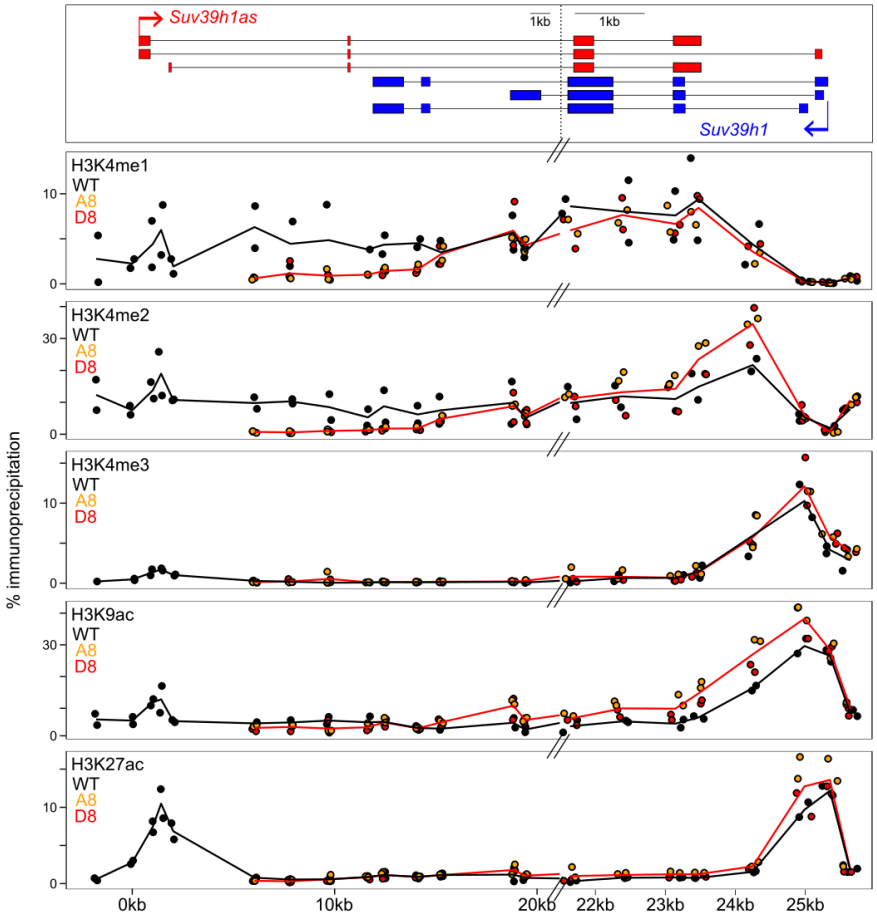

Figure 4: *Suv39h1as* triggers complex chromatin changes across the locus. Chromatin immunoprecipitation profile of H3K4me1, H3K4me2, H3K4me3, H3K9ac and H3K27ac, as indicated, across *Suv39h1*/*Suv39h1as* locus in WT (black) and *Suv39h1as*-mutant cells (A8, yellow dots; D8, red dots; the red line represents the average of all data points for mutant clones). The X-axis represents genomic distances in kb with respect to the *Suv39h1as* transcription start site, as schematized on top. Note a break on the scale of the genomic coordinates at around X=21kb. For the analysis of the locus-wide effects of the loss of *Suv39h1as* on H3K4me1 and me2, all values obtained with primer pairs located between coordinates +6 and +15 were considered (t test $p<0.001$); for the effects measured at the promoter region, the position showing the highest difference for each histone mark was used (t test $p<0.05$ for H3K4me2/me3, H3K9ac and H3K27ac).

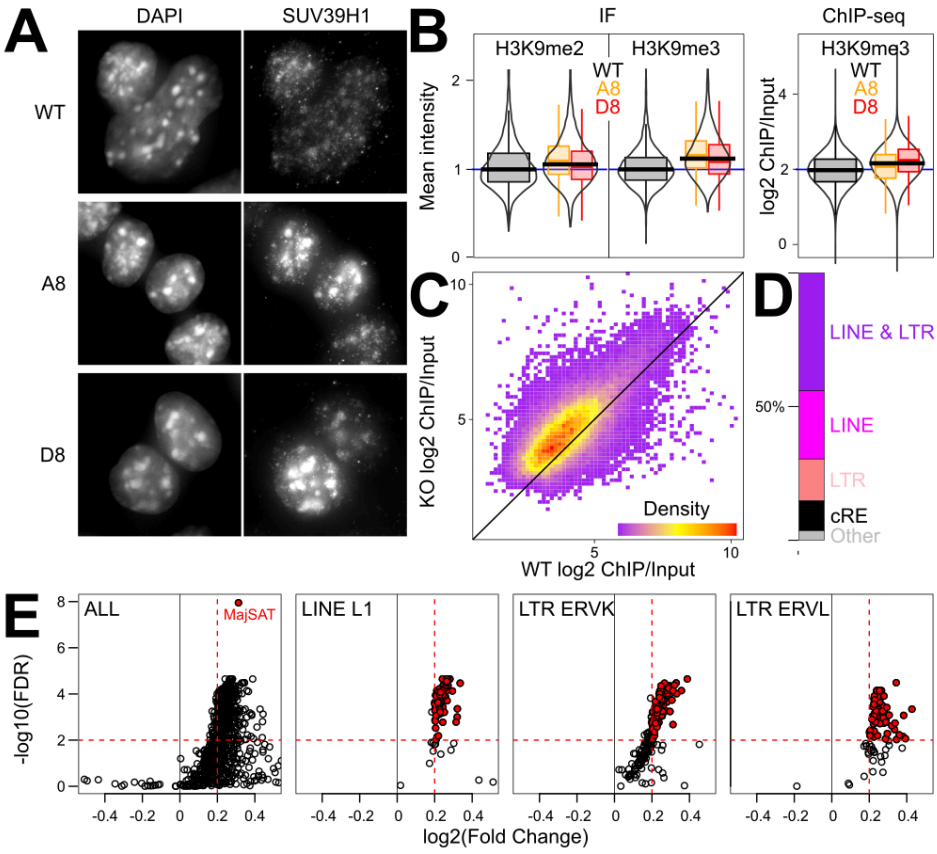

Figure 5: Global increase of H3K9 methylation in *Suv39h1as* mutant cells. (A) Representative SUV39H1 immunofluorescence of WT and *Suv39h1*-mutant ES cells (A8 and D8). **(B)** Violin and boxplots (median; 25-75% percentiles; error bars) of H3K9 methylation levels measured by immunofluorescence (left) or ChIP-seq (right). Immunofluorescence data shows relative mean intensity values of WT (black; n=12881 for H3K9me2 and n=12053 for H3K9me3) or mutant cells (A8, yellow, n=3553 cells for H3K9me2 and 2081 for H3K9me3; D8, red, n=5050 cells for H3K9me2 and 2641 for H3K9me3). KS tests were performed to compare WT and mutant cells ($p<10^{-8}$ for both marks and cell clones). ChIP-seq data shows log2 fold change of H3K9me3 over input, calculated after normalising both values to internal *Drosphila* spike in controls, for all the regions identified as H3K9me3-enriched in either WT or mutant clones. Differences between WT and mutant cells were evaluated with KS tests ($p<10^{-15}$ for both clones). (**C**) Scatter plot (X-axis: H3K9me3 levels in WT cells; Y:axis: mean H3K9me3 levels of the two mutant clones) corresponding to the data shown in (B). (**D**) Proportion of H3K9me3-enriched regions overlapping with both LINE and LTR retrotransposons or with only one of the two families or with cis-regulatory elements[54] (cRE) or with none of the above (Other). (**E**) Global analysis of repetitive elements[53], visualised as a volcano plot (X-axis: log2 fold change between mean H3K9me3 levels in mutant clones and WT cells; Y-axis: -log10(FDR); both calculated with DESeq2[55] and considering Drosophila spike in controls. The first panel shows all repeat families, with major Satellites highlighted in red. The three following panels display selected families, as indicated, with red points highlighting elements with FDR<0.01 and log2(FC)>0.2.

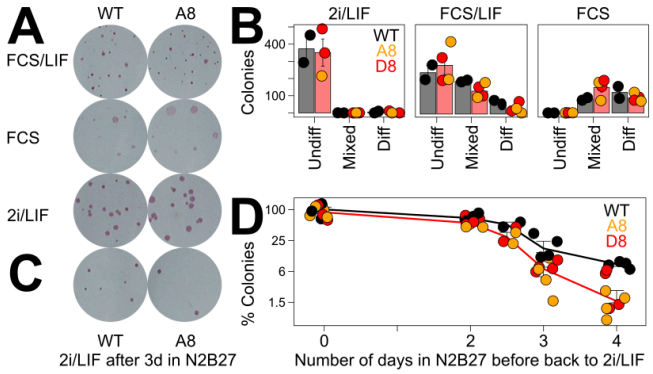

Figure 6: Accelerated commitment into differentiation in the absence of *Suv39h1as*. (A) Representative alkaline-phosphatase staining of ES cell colonies cultured as indicated. **(B)** Number of WT or *Suv39h1as*-mutant (A8, orange points; D8, red points) colonies characterized as undifferentiated, mixed or differentiated after culturing them as indicated. Each dot represents an independent replicate and the bar and error bars the corresponding means (black for WT and red for the mean of all data points for mutant clones) and standard errors. **(C)** Alkaline-phosphatase staining of ES cell colonies cultured in 2i/LIF after 3 days in N2B27 for WT and *Suv39h1as*-mutant cells (A8). **(D)** Percentage of alkaline-phosphatase positive colonies cultured in 2i/LIF after differentiating them for the indicated number of days (X-axis) in N2B27. D0, undifferentiated cells were set as 100%. Each dot represents an independent replicate (WT, black; *Suv39h1as*-mutant clones in orange, A8, and red, D8) and the line the corresponding mean and standard error (all mutant data points were averaged to obtain the red line). Differences between WT and the mean of the two mutant clones were evaluated with Mann-Whitney tests using raw colony numbers (p=0.0666, 0.0020 and 0.0041 for days 2.5, 3 and 4, respectively)

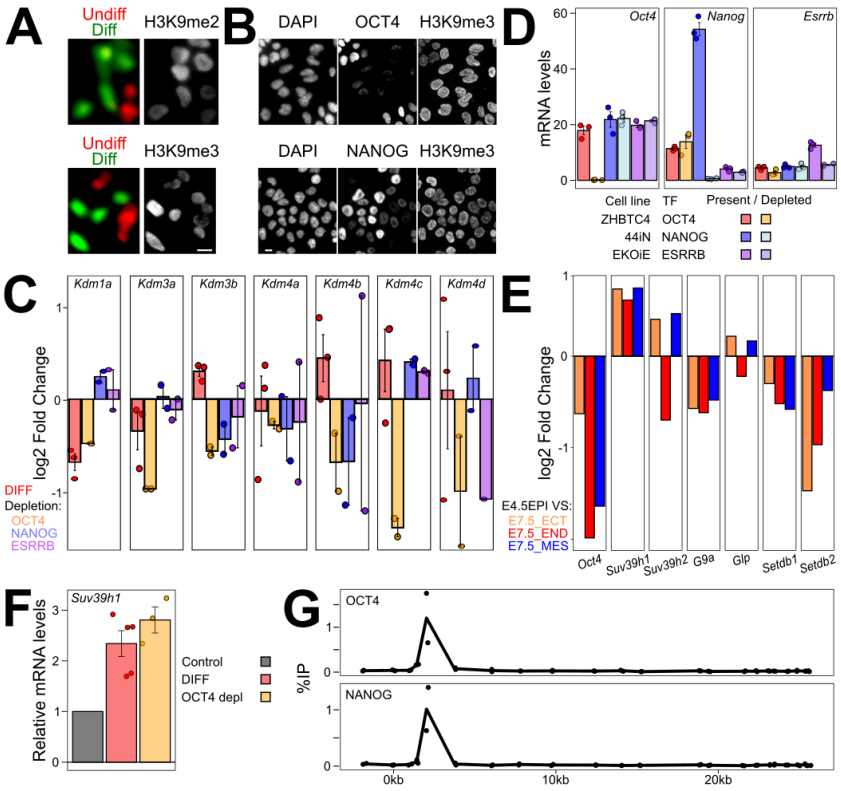

Supplementary figure 1: Additional information for the correlations existing between pluripotency, OCT4 and *Suv39h1*. (A) Illustrative immunofluorescence of H3K9me2 and H3K9me3 in undifferentiated and differentiating ES cells stained and imaged together after independently labelling them with different fluorochromes. **(B)** Illustrative immunofluorescence of OCT4-H3K9me3 or NANOG-H3K9me3 in cultures presenting spontaneously differentiating ES cells. **(C)** Expression of H3K9 de-methylases presented as in Fig.1B **(D)** Expression of *Oct4*, *Nanog* or *Esrrb* upon inducing their depletion in specific dox-inducible knock-out lines. Note in EKOiE the remnant expression of Esrrb produces a truncated, non-functional protein[24]. Each dot represents an independent replicate and the bar the corresponding mean and standard error. **(E)** Log2 fold change of *Oct4* and H3K9 methylases between the three main germ layers of E7.5 embryos and the pluripotent epiblast of E4.5 embryos[27]. **(F)** RT-qPCR validation of *Suv39h1* overexpression upon differentiation (DIFF, 3 days without LIF, red) or upon OCT4 depletion (24h, orange). Each dot represents an independent replicate and the histogram the corresponding mean and standard error. **(G)** ChIP-qPCR validation of OCT4 and NANOG binding at the promoter region of *Suv39h1as* in WT.

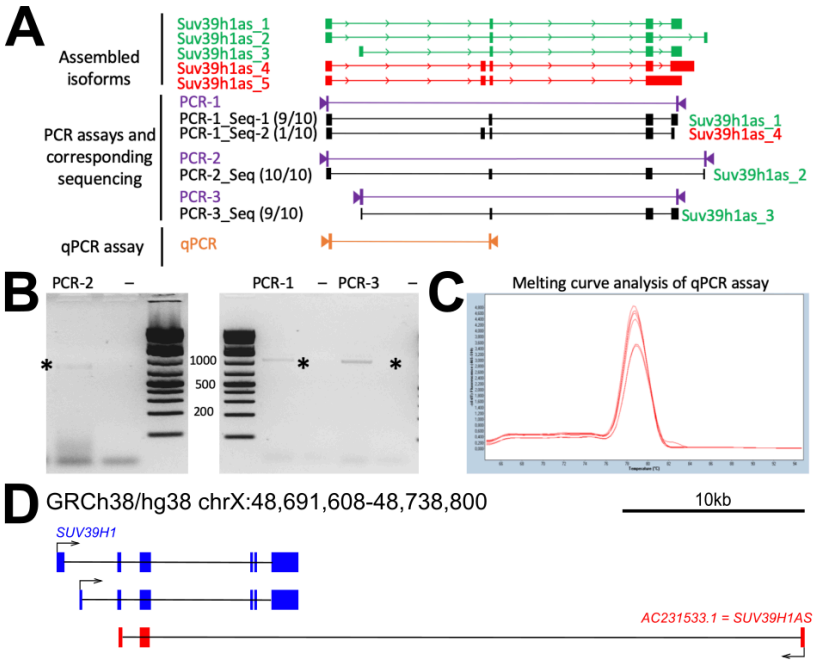

Supplementary figure 2: Additional information on *Suv39h1as* isoforms and conservation. (A-C) *Suv39h1as* isoforms identified in silico using de novo transcript assembly are shown in **(A)** (green and red). Isoforms 1, 2, 3 and 4 were confirmed by cDNA cloning and sequencing, using the primers shown in purple and transforming bacteria with the PCR products shown in **(B)**. However, isoform 4 was found in only 1 out of 10 bacterial colonies, as indicated in (A), and was thus excluded from the final selection. Isoform 5 was never cloned. Moreover, since it has the same 5' end than isoforms 1 and 2, but with an additional small exon, we used melting curve analysis of qPCR reactions **(C)** using primers shown in orange (A), to test whether two different molecular species were amplified. Since this was not the case, isoform 5 was excluded. **(D)** Schematic representation of the *SUV39H1*/ *SUV39H1as* locus in the human genome (Gencode V36 assembly).

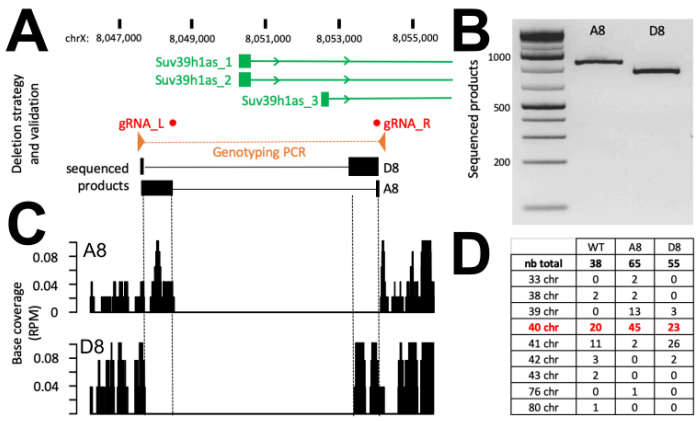

	WT	A8	D8
nb total	38	65	55
33 chr	0	2	0
38 chr	2	2	0
39 chr	0	13	3
40 chr	20	45	23
41 chr	11	2	26
42 chr	3	0	2
43 chr	2	0	0
76 chr	0	1	0
80 chr	1	0	0

Supplementary Figure 3: Additional information on *Suv39h1as* mutant clones. (A) Schematic representation of the *Suv39h1as* promoter region with the gRNAs used for the deletion and the location of the primers used for validation. **(B)** PCR products using the primers shown in (A) in the two mutant clones. **(C)** Sequencing of sonicated genomic DNA to fully map the deletion boundaries. Overall, these analyses show that the precisely expected deletion was observed for A8 (5.5kb); D8 showed a 5.7kb deletion exhibiting a shift of 700bp compared to A8 but encompassing both *Suv39h1as* promoters. **(D)** Karyotype results for both clones, showing that A8 exhibits a normal karyotype and D8 presents 50% of cells with an extra chromosome.

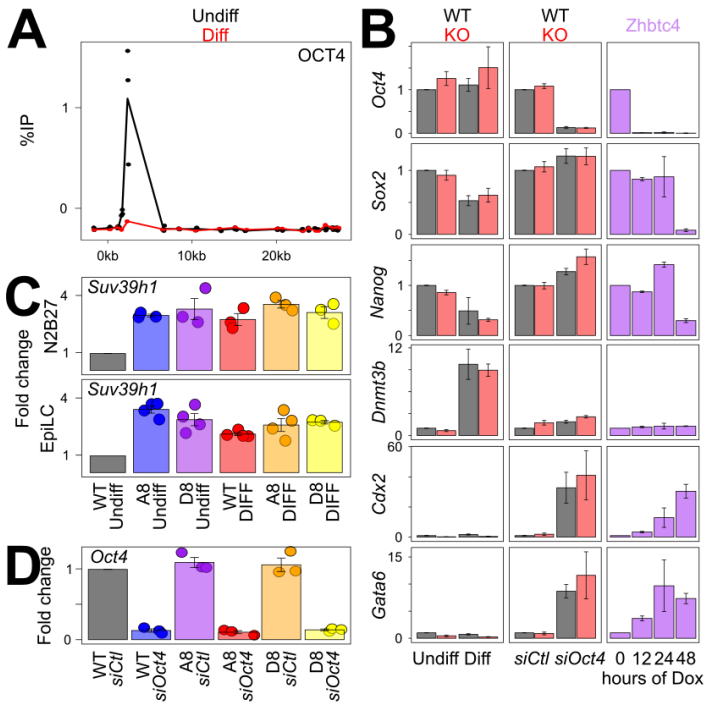

Supplementary Figure 4: Additional information and controls of differentiating ES cells. (A) ChIP-qPCR of OCT4 presented as in Fig.S1 but including a differentiating ES cell sample (3 days without LIF). **(B)** Gene expression marker analysis in the indicated cell lines (top) and conditions (bottom). **(C)** RT-qPCR confirmation of the lack of increased *Suv39h1* upregulation in differentiated *Suv39h1as*-mutant cells obtained by N2B27 or EpiLC assays as compared to WT cells. **(D)** RT-qPCR confirmation of *Oct4* knock-down in WT and *Suv39h1as*-mutant cells.

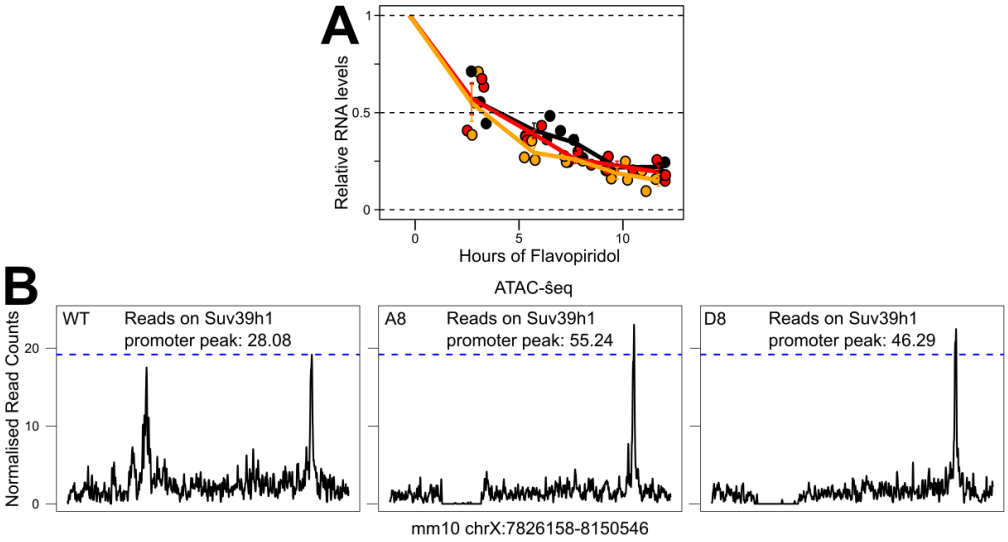

Supplementary Figure 5: Additional support to the transcriptional induction of *Suv39h1* in *Suv39h1as* mutants. **(A)** Analysis of *Suv39h1* mRNA half-life in WT (black) and *Suv39h1as*-mutant cells (A8, orange; D8, red), performed and presented as in Fig. 2A. **(B)** Accessibility profile across the *Suv39h1*/*Suv39h1as* locus in WT and mutant clones. The blue line denotes the highest height measured in WT cells. The number of normalised reads on the peak identified by MACS2 at the *Suv39h1* promoter are indicated in each panel (Table S2).

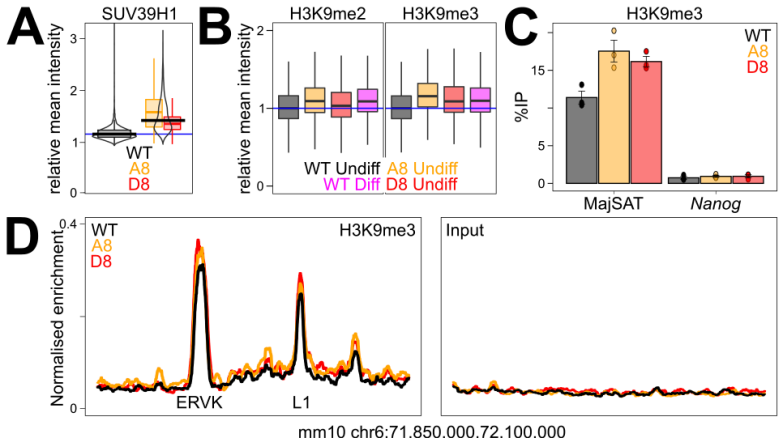

Supplementary Figure 6: Additional data supporting the increase of H3K9 methylation in *Suv39h1as* mutant cells. (A) Violin and box-plots showing immunofluorescence quantification of SUV39H1 mean intensity in WT (black; n= 4048 cells) and mutant cells (A8 – orange; n= 4949 cells and D8 – red; n= 4448 cells). **(B)** Box-plots directly comparing data of Fig.5B with Fig.1A, underscoring the physiological increase of H3K9 methylation in undifferentiated *Suv39h1as* mutant clones. **(C)** ChIP-qPCR of H3K9me3 at Major Satellites and a negative control, the -5kb enhancer of *Nanog*. **(D)** Normalised enrichment of H3K9me3 across the indicated region and corresponding input profiles, in WT and mutant cells. The position of nearly full-length ERVK and L1 elements is indicated.

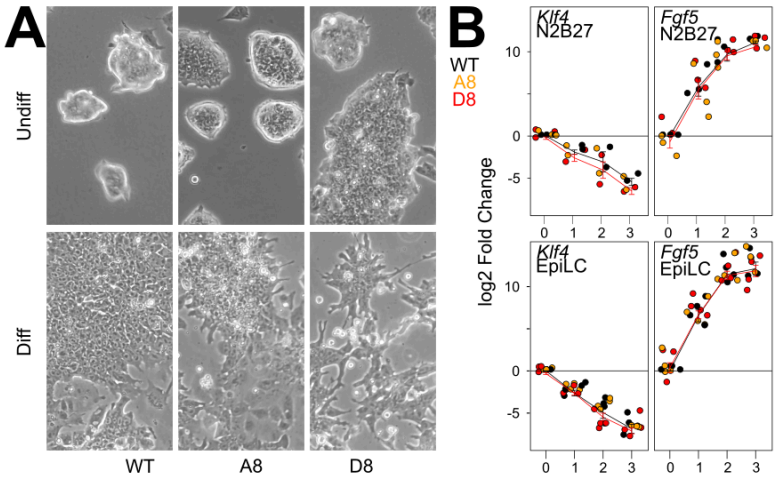

Supplementary Figure 7: Additional information on the differentiation capacity of *Suv39h1as* mutants. (A) Representative photomicrographs of undifferentiated and differentiating WT and mutant cells. **(B)** RT-qPCR analysis of ES (*Klf4*) and differentiation (*Fgf5*) markers during differentiation in N2B27 or in EpiLC conditions, as indicated, in WT and in *Suv39h1as*-mutant cells.

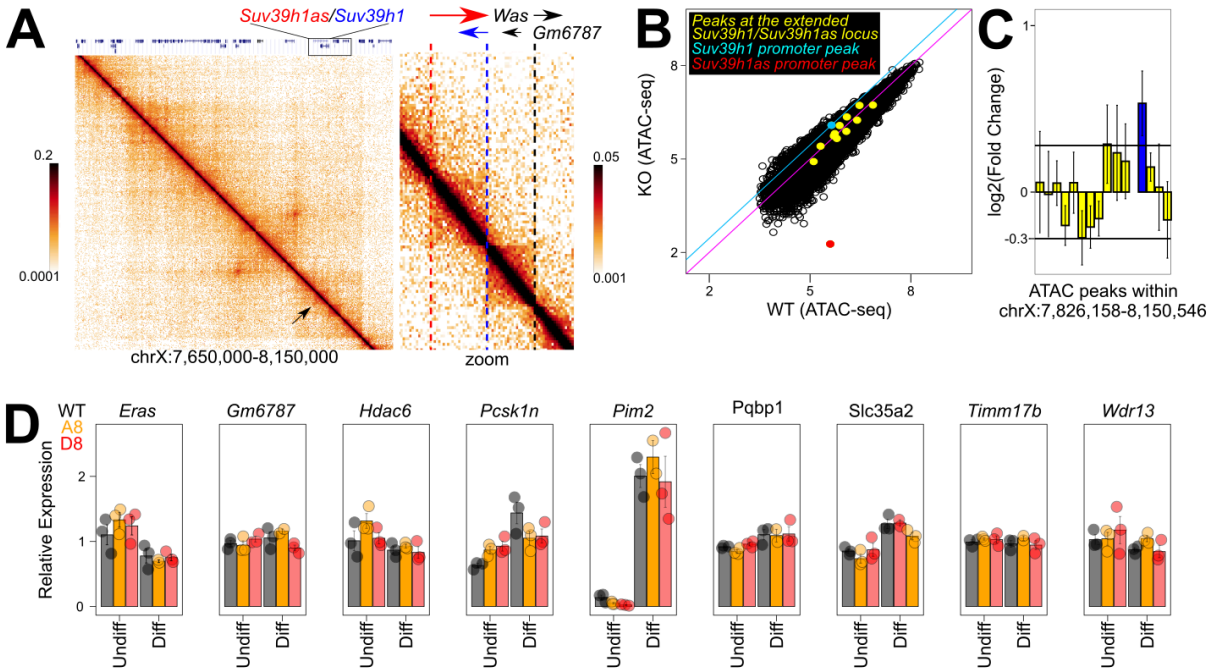

Supplementary Figure 8: Additional data supporting the local effects of *Suv39h1as* deletion. (A) MicroC data visualised on the Higlass.io browser (Hsieh et al. 2019). On the left, a large 500Mb long region; the arrow indicates the position of the *Suv39h1*/*Suv39h1as* locus. On the right, closer visualisation of the *Suv39h1*/*Suv39h1as* locus. **(B)** Scatter plot of Drosophila spike normalised accessibility in WT (X-axis) and mutant *Suv39h1as* cells (Y-axis; mean of both A8 and D8 clones), at all identified ATAC-seq peaks in either condition (Table S2). Coloured points correspond to peaks identified in the extended *Suv39h1*/*Suv39h1as* locus – coordinates shown in (C) – with red corresponding to the *Suv39h1as* promoter region and blue to the *Suv39h1* promoter; the blue diagonal highlights that no other local peak surpasses the increase seen for *Suv39h1* promoter. **(C)** Same data as in (B) but plotted as a log2 fold-change of mutant over WT cells. **(D)** Expression analysis of all genes sharing at least one enhancer.

Supplementary Table S1: This table reports gene expression counts of undifferentiated and differentiating ES cells as well as of Dox-inducible depletions of *Oct4*, *Nanog* and *Esrrb*.
Supplementary Table S2: This table reports ATAC-seq data at all peaks identified.
Supplementary Table S3: This table reports H3K9me3 data at all identified enriched regions.
Supplementary Table S4: This table describes H3K9me3 data at all analysed repetitive elements.
Supplementary Table S5: This table describes several reagents (primers, gRNAs, antibodies).

References

1. Li, E. Chromatin modification and epigenetic reprogramming in mammalian development. Nat Rev Genet 3, 662-673 (2002).
2. Allshire, R. C. & Madhani, H. D. Ten principles of heterochromatin formation and function. Nat Rev Mol Cell Biol 19, 229–244 (2018).
3. Trojer, P. & Reinberg, D. Facultative Heterochromatin: Is There a Distinctive Molecular Signature? Molecular Cell 28, 1–13 (2007).
4. Saksouk, N., Simboeck, E. & Déjardin, J. Constitutive heterochromatin formation and transcription in mammals. Epigenetics & Chromatin 8, 3 (2015).
5. Liu, J., Ali, M. & Zhou, Q. Establishment and evolution of heterochromatin. Annals of the New York Academy of Sciences 1476, 59–77 (2020).
6. Tosolini, M. et al. Contrasting epigenetic states of heterochromatin in the different types of mouse pluripotent stem cells. Scientific Reports 8, 5776 (2018).
7. Walter, M., Teissandier, A., Pérez-Palacios, R. & Bourc'his, D. An epigenetic switch ensures transposon repression upon dynamic loss of DNA methylation in embryonic stem cells. Elife 5, (2016).
8. Johnson, W. L. et al. RNA-dependent stabilization of SUV39H1 at constitutive heterochromatin. eLife 6, e25299 (2017).
9. Nicetto, D. & Zaret, K. Role of H3K9me3 heterochromatin in cell identity establishment and maintenance. Curr Opin Genet Dev, 55, 1-10 (2019).
10. Janssen, A., Colmenares, S. U. & Karpen, G. H. Heterochromatin: Guardian of the Genome. Annu. Rev. Cell Dev. Biol. 34, 265–288 (2018).
11. Dodge, J. E., Kang, Y.-K., Beppu, H., Lei, H. & Li, E. Histone H3-K9 Methyltransferase ESET Is Essential for Early Development. MCB 24, 2478–2486 (2004).
12. Tachibana, M. et al. G9a histone methyltransferase plays a dominant role in euchromatic histone H3 lysine 9 methylation and is essential for early embryogenesis. Genes Dev 16, 1779–1791 (2002).
13. Zhang, Y.-L. et al. DCAF13 promotes pluripotency by negatively regulating SUV39H1 stability during early embryonic development. EMBO J. 37, (2018).
14. Burton, A. et al. Heterochromatin establishment during early mammalian development is regulated by pericentromeric RNA and characterized by non-repressive H3K9me3. Nat Cell Biol 22, 767–778 (2020).
15. Bernstein, B. E. et al. A bivalent chromatin structure marks key developmental genes in embryonic stem cells. Cell 125, 315–326 (2006).

16. Mikkelsen, T. S. et al. Genome-wide maps of chromatin state in pluripotent and lineage-committed cells. Nature 448, 553–560 (2007).
17. Wen, B. et al. Large histone H3 lysine 9 dimethylated chromatin blocks distinguish differentiated from embryonic stem cells. Nat Genet 41, 246–250 (2009).
18. Sridharan, R. et al. Proteomic and genomic approaches reveal critical functions of H3K9 methylation and heterochromatin protein-1γ in reprogramming to pluripotency. Nat Cell Biol 15, 872–882 (2013).
19. Wei, J. et al. KDM4B-mediated reduction of H3K9me3 and H3K36me3 levels improves somatic cell reprogramming into pluripotency. Sci Rep 7, 7514 (2017).
20. Becker, J. S., Nicetto, D. & Zaret, K. S. H3K9me3-Dependent Heterochromatin: Barrier to Cell Fate Changes. Trends in Genetics 32, 29–41 (2016).
21. Evsikov, A.V. et al. Cracking the egg: molecular dynamics and evolutionary aspects of the transition from the fully grown oocyte to embryo. Genes Dev. 20(19):2713-27 (2006).
22. Staněk, D. Long non-coding RNAs and splicing. Essays Biochem EBC20200087 (2021)
23. Heurtier, V. et al. The molecular logic of Nanog-induced self-renewal in mouse embryonic stem cells. Nat Commun 10, 1109 (2019).
24. Festuccia, N. et al. Mitotic binding of Esrrb marks key regulatory regions of the pluripotency network. Nat Cell Biol. 18(11):1139-1148 (2016).
25. Niwa, H., Miyazaki, J. & Smith, A. G. Quantitative expression of Oct-3/4 defines differentiation, dedifferentiation or self-renewal of ES cells. Nat. Genet. 24, 372–376 (2000).
26. Navarro, P. et al. OCT4/SOX2-independent Nanog autorepression modulates heterogeneous Nanog gene expression in mouse ES cells. EMBO Journal 31, 4547–4562 (2012).
27. Argelaguet, R. et al. Multi-omics profiling of mouse gastrulation at single-cell resolution. Nature 576(7787):487-491 (2019).
28. Festuccia, N. et al. Transcription factor activity and nucleosome organization in mitosis. Genome Research 29, 250-260 (2019).
29. Wang, L. et al. CPAT: Coding-Potential Assessment Tool using an alignment-free logistic regression model. Nucleic Acids Res 41, e74 (2013).
30. Kang, Y.-J. et al. CPC2: a fast and accurate coding potential calculator based on sequence intrinsic features. Nucleic Acids Res 45, W12–W16 (2017).
31. Deng, Q. et al. Single-Cell RNA-Seq Reveals Dynamic, Random Monoallelic Gene Expression in Mammalian Cells. Science 343, 193–196 (2014).
32. Boroviak, T. et al. Lineage-Specific Profiling Delineates the Emergence and Progression of Naive Pluripotency in Mammalian Embryogenesis. Dev Cell. 35(3):366-82 (2015).

33. King, H.W. & Klose, R.J. The pioneer factor OCT4 requires the chromatin remodeller BRG1 to support gene regulatory element function in mouse embryonic stem cells. Elife. 6:e22631 (2017).
34. Bates, L.E., Alves M.R.P. & Silva J.C.R. Auxin-degron system identifies immediate mechanisms of OCT4. Stem Cell Reports. 16(7):1818-1831 (2021).
35. Ohhata, T. et al. Dynamics of transcription-mediated conversion from euchromatin to facultative heterochromatin at the Xist promoter by Tsix. Cell Reports 34, 108912 (2021).
36. Navarro, P. et al. Tsix transcription across the Xist gene alters chromatin conformation without affecting Xist transcription: implications for X-chromosome inactivation. Genes Dev. 19, 1474–1484 (2005).
37. Navarro, P. et al. Tsix-mediated epigenetic switch of a CTCF-flanked region of the Xist promoter determines the Xist transcription program. Genes & Development 20, 2787–2792 (2006).
38. Santos-Rosa, H. et al. Active genes are tri-methylated at K4 of histone H3. Nature 419, 407–411 (2002).
39. Wang, C. et al. Reprogramming of H3K9me3-dependent heterochromatin during mammalian embryo development. Nat Cell Biol 20, 620–631 (2018).
40. Nicetto, D. et al. H3K9me3-heterochromatin loss at protein-coding genes enables developmental lineage specification. Science 363(6424):294-297 (2019).
41. McCarthy, R.L. et al. Diverse heterochromatin-associated proteins repress distinct classes of genes and repetitive elements. Nat Cell Biol. 23(8):905-914 (2021).
42. Kalkan, T. et al. Tracking the embryonic stem cell transition from ground state pluripotency. Development 144, 1221–1234 (2017).
43. Carlini, V., Policarpi, C. & Hackett JA. Epigenetic inheritance is gated by naïve pluripotency and Dppa2. EMBO J. 41(7):e108677 (2022).
44. Torres-Padilla, M.-E. & Chambers, I. Transcription factor heterogeneity in pluripotent stem cells: a stochastic advantage. Development 141, 2173–2181 (2014).
45. Katayama, S. et al. Antisense transcription in the mammalian transcriptome. Science 309, 1564–1566 (2005).
46. Cho, S.W. et al. Promoter of lncRNA Gene PVT1 Is a Tumor-Suppressor DNA Boundary Element. Cell. 173(6):1398-1412.e22 (2018).
47. González-Ramírez, M. et al. Differential contribution to gene expression prediction of histone modifications at enhancers or promoters. PLoS Comput Biol. 17(9):e1009368 (2021).
48. Prescott, E. M. & Proudfoot, N. J. Transcriptional collision between convergent genes in budding yeast. Proc Natl Acad Sci U S A 99, 8796–8801 (2002).

1 49. Hastings, M. L. et al. Expression of the thyroid hormone receptor gene, erbAalpha, in B
2 lymphocytes: alternative mRNA processing is independent of differentiation but correlates
3 with antisense RNA levels. Nucleic Acids Res 25, 4296–4300 (1997).
4 50. Peters, A. H. F. M. et al. Loss of the Suv39h Histone Methyltransferases Impairs
5 Mammalian Heterochromatin and Genome Stability. Cell 107, 323–337 (2001).
6 51. Festuccia, N., Gonzalez, I. & Navarro, P. The Epigenetic Paradox of Pluripotent ES Cells.
7 Journal of Molecular Biology 429, 1476–1503 (2017).
8 52. Liu, H., Kim, J.-M. & Aoki, F. Regulation of histone H3 lysine 9 methylation in oocytes and
9 early pre-implantation embryos. Development 131, 2269–2280 (2004).
10 53. Criscione, S.W. et al. Transcriptional landscape of repetitive elements in normal and cancer
11 human cells. BMC Genomics. 15:583 (2014).
12 54. Ernst, J. & Kellis, M. ChromHMM: automating chromatin-state discovery and characterization.
13 Nat Methods. 9(3):215-6 (2012).
14 55. Love, M.I., Huber, W. & Anders, S. Moderated estimation of fold change and dispersion for
15 RNA-seq data with DESeq2. Genome Biol. 15(12):550 (2014).